Experimental and Thermodynamic Study of Nickel-Base Alloys containing Chromium Carbides: Part II -Study of the Sub-Surface Characteristics of Ni-30%wt.Cr-xC Alloys oxidized at High Temperature using Thermodynamic Calculations

P. Berthod

Experimental and Thermodynamic Study of Nickel-Base Alloys containing Chromium Carbides:
Part II - Study of the Sub-Surface Characteristics of Ni-30%wt.Cr-xC Alloys oxidized at High Temperature using Thermodynamic Calculations

P. Berthod *
Laboratoire de Chimie du Solide Minéral (UMR 7555),
Faculté des Sciences et Techniques, UHP Nancy 1, Nancy - Université
BP 239, 54506 Vandoeuvre-lès-Nancy – France
* Corresponding author's e-mail: patrice.berthod@centraliens-lille.org
* Correspond. author's phone number: (33)383684666 and fax number: (33)383684611

Post-print version of the article *Calphad, Vol. 32, pp. 492-499 (2008); doi:10.1016/j.calphad.2008.06.005*

Abstract. Six ternary Ni-30 wt.%Cr-xC alloys (x = 0.2 to 2.0) were oxidized at 1,000, 1,100 and 1,200°C. For several of them, the sub-surface was studied with accuracy by division into several successive parts for local measurements of carbide fractions by image analysis. Additionally thermodynamic calculations were performed for local analysis of the samples. By these means, the outer carbide-free zone and the inner zone enriched in carbides were characterized, with special attention to both local carbon contents and local solidus temperatures. Profiles of carbon contents (and thereafter of local solidus temperatures) across the zone affected by oxidation were obtained by thermodynamic calculations. The content of carbon still present in the carbide-free zone is necessarily very low. The carbon content in the zone enriched in carbides is higher than in the bulk. The loss of carbon leads to a higher refractoriness for the carbide-free zone, which could protect the bulk against fast oxidation if it becomes partially molten because of a sudden increase in temperature in service.
Keywords: Nickel-based alloys; High temperature oxidation; Thermodynamic modeling; Carbon; Sub-surface refractoriness

1. Introduction

When exposed to high temperature in service, metallic alloys are subjected to microstructure transformations in the bulk which can affect the mechanical properties [1–3]. Surface and/or sub-surface modifications also occur when the atmosphere contains oxidizing gases. Indeed an external oxide scale grows on the surface, while internal oxidation sometimes also occurs. Simultaneously, the metallurgical state can change in the sub-surface across a depth of several tens or hundreds micrometers. There is usually a depletion of elements involved in the growth of the external oxide scale, and sometimes voids appear in the sub-surface [4–5]. In the case of alloys strengthened by carbides, these may disappear in a zone which grows from the external surface, especially if these carbides contain an element easy to oxidize such as chromium in the M_7C_3 or $M_{23}C_6$ carbides, or tantalum and tungsten in the MC carbides. The carbon released by the reacting carbides can be either oxidized or it remains in the alloy. For the second case, it was previously demonstrated, for Ni-based or Co-based Ta-containing alloys, that the carbon content in the carbide-free zone is equal to zero, or at least is necessarily very low [6–8]. During oxidation, the carbon atoms which were initially present diffused deeper into the alloy. They promoted the coarsening of the

existing carbides, a modification of their composition, and/or the precipitation of new ones.

In this work the seven Ni – 30 wt.%Cr – x %C alloys (x = 0, 0.2, 0.4, 0.8, 1.2, 1.6 and 2.0 wt.%C), for which the bulk microstructures at high temperature were studied in the first part of this work [9], were subjected to high temperature oxidation. Their sub-surface states were studied following a similar procedure as the one previously applied for more complex alloys [6–8], but with an improved accuracy since it was here attempted to more precisely specify the new distribution of carbon across the alloy zone affected by oxidation. Indeed, the carbide fractions determined by image analysis measurements and the carbon contents deduced by thermodynamic calculations, were plotted versus the distance from the external surface. The refractoriness of the carbide-free zone, and of the carbide-enriched zone which sometimes exists between the carbide-free zone and the bulk, were also estimated.

2. Experimental method

2.1. Metallography

Three {10 × 10 × 3 mm^3} samples per cast alloy were prepared by cutting and polishing with abrasive paper (1,200 grit). Thereafter, they were oxidized in air at 1,000, 1,100 and 1,200°C during 50 hours in a resistive furnace. Finally, the oxidized samples were cut, embedded in resin, and polished in order to get a mirror-like surface ready for metallographic observations and measurements.

The sub-surfaces of all the samples were examined using a Scanning Electron Microscope (SEM) Philips XL30 in the Back Scattered Electrons mode (BSE) with a 20 kV acceleration voltage. This allowed identifying the samples displaying one of the possible microstructure phenomena involving carbon:

- coarsening of the existing carbides,
- change of their gray level, i.e. of their chemical composition,
- solid state precipitation of new carbides in an area separating the carbide-free zone and the not modified bulk.

Three SEM micrographs in BSE mode and at ×250 magnitude were taken on the sub-surface for each sample displaying these phenomena, at three different locations (randomly chosen). The BSE mode allowed distinguishing the matrix (gray) and the chromium carbides (darker than matrix). Each micrograph was visualized and "electronically cut", using the Microsoft Photo Editor software, in nine strips (numbered from 0 to 8); all these strips are parallel to the oxidized surface and they are situated at an increasing depth when the number increases from 0 to 8. Each of them covers a real area of approximately 30µm (width or depth) x 400µm (length) in the alloy.

Each strip was analyzed using the Adobe Photoshop CS software to measure the surface fraction of carbides by image analysis. Initially, the rating of the adequate gray level was done for the four inner strips (numbers from "5" to "8"), in order to allow reaching (by performing image analysis) the volume fraction calculated by Thermo-Calc for the bulk chemical composition. These strips "5" to "8" were supposed to be sufficiently far away from the external surface to cover a part of alloy which was not affected by oxidation. These strips represented microstructures totally similar to the bulk one. This value of gray level was then used for all the strips ("0" to "8") cut in the

same micrograph, for the measurement of the surface fractions of carbides. Indeed, it could be reasonably assumed that the average rating done for the strips "5" to "8" was effectively valid for all the strips since they belong to the same micrograph. In contrast, all this procedure must be followed again for the second and the third micrographs taken on the same sample, since brightness and contrast may be different for them, because of a possible variation of the current in the electrons-emitting tungsten filament of the SEM.

Thus, three values of carbide surface fraction were obtained for each depth from the external surface (15, 45, 75, … µm, values of the depth of the center of each strip; e.g. 15µm = 30µm / 2 for the strip "0"). For each depth this allowed the calculation of the average value and of the standard deviation, and it was possible to plot a curve or a histogram representing the evolution of the carbide surface fraction versus the depth. The surface fractions measured on the strip "0" were corrected since the gray level sometimes led to the detection of internal oxides or voids, in addition to the real carbides. This correction was achieved by estimating the fraction of voids and oxides among the selected pixels, and by multiplying the surface fraction by a correcting factor.

Profiles of the chromium content across the zone affected by oxidation were performed, using a Cameca SX100 microprobe with the Wavelength Dispersion Spectrometry mode (WDS). It was not possible to get such profiles for carbon because of low concentration in matrix and low atomic mass.

2.2. Thermodynamic calculations

The average values of the measured surface fractions for each depth, which were supposed being close to the volume fractions, were first converted into weight fractions according to equation (1):

$$f_w[\varphi_j] = (\rho_{\varphi j} \times f_v[\varphi j]) \,/\, \sum_i (\rho_{\varphi i} \times f_v[\varphi i]) \qquad (1)$$

in which $f_w[\varphi j]$, $f_v[\varphi j]$ and $\rho_{\varphi j}$ are respectively the weight fraction, the volume fraction and the density of the phase φ_j. The values of densities are 8.12 g cm^{-3} for matrix and 6.941 g cm^{-3} for the Cr_7C_3 carbides [10]. Thereafter the mass of carbide was calculated from these weight fractions for a given mass of alloy (e.g. 100g). They were then divided by the molar weight of the Cr_7C_3 carbides (400g/mol) in order to obtain the number of moles of Cr_7C_3 for the given mass of alloy.

Calculations were performed with the Thermo-Calc software [11] and the same database as in the first part of this work [9] (containing the systems Ni-Cr, Ni-C, Cr-C and Ni-Cr-C [12–15]). Calculations were used to determine the carbon content which led to the number of moles of carbide, for each depth.

Finally, knowing the distribution of the carbon content (from thermodynamic calculations) and of chromium content (WDS profile in the carbide-free zone and 30 wt.%Cr deeper), it was possible to calculate the local solidus temperature for each depth using Thermo-Calc.

3. Results

3.1. Analysis of the alloys containing an internal zone enriched in carbides

Only some of the samples display a phenomenon of carbide coarsening or of carbide precipitation, in an area separating the carbide-free zone and the bulk. These samples are Ni02, Ni04, Ni08 and Ni12, all oxidized at 1,000°C, and also Ni12 oxidized at 1,100°C. Figure 1 presents four examples of such sub-surface microstructures. For comparison, two other samples, in which neither carbide coarsening nor precipitation of carbides occurred, are added.

These alloys were analyzed according to the method described above, which can be illustrated by Figure 2 for one of the alloys affected by a coarsening of carbides near the external surface (Ni04 alloy oxidized at 1,000°C). In this one, a sub-surface SEM micrograph (top) was sectioned in nine strips (bottom, left) numbered from “0” (the more external one) to “8” (the more internal one). Several gray levels of detection were tested on the strips from “5” to “8” until the theoretical surface fraction of carbides (deduced from the mass fraction calculated by Thermo-Calc) was reached. The better gray level was then applied to each strip (bottom, right), before their analysis for obtaining their surface fraction of carbides (values given just under each digitalized picture strip). Since the first strip (“0”) also contains internal oxides and voids which were partially detected together with carbides, the surface fractions were corrected by multiplying their values by a correcting factor lower than 1, before further calculations. For instance this factor is simply zero in the case of Figure 2 since the strip “0” corresponds to the carbide-free zone and only contains internal oxides and voids (the 9.00% value was then replaced by 0%). Knowing the nature and the average surface fraction of the carbide (which was supposed to be almost equal to the volume fraction), the carbide mass fractions can be deduced.

3.2. Determination of the carbon distribution using thermodynamic calculations

The carbon content, which cannot be directly measured by microanalysis, can be determined using Thermo-Calc, but the local chromium content must be known first. This element diffuses towards the external surface during high temperature oxidation, since it is involved in the formation of the external protective scale of chromia Cr_2O_3. This outward diffusion of chromium led to a chromium depletion in the sub-surface, and WDS chromium profiles must be performed perpendicular to the external surface (example in Figure 3). The obtained chromium profiles and the absence of carbides show that the chromium content varies across the carbide-free zone essentially. Indeed, the loss of chromium in the zones which still contain carbides is much lower: the loss of Cr in matrix is slightly lower than in the carbide-free zone (as shown by WDS profiles) and the carbides - and then the chromium that they contain - are still present with a higher fraction (zone with coarsened carbides) or with seemingly the same fraction (zone where carbides seem unchanged). It can be then assumed that the chromium content remains close to the initial value of 30 wt.% Cr, as verified by global EDS measurements in these zones.

Considering a mass of 100g of alloy, the weight content of carbon leading to the number of moles of Cr_7C_3 carbides with Thermo-Calc, was then determined in each carbides-containing strip (values given in the last column of Table 1).

3.3. Carbon weight content profiles and balance sheets

The evolution of the surface (or volume) fraction of carbides and of the mass fraction of carbides, versus the depth in the alloy from the external surface, are plotted in the graphs displayed in the first column of Figure 4 for three of the five studied samples. After the first strip in which carbides have partially disappeared, a local increase in carbide fraction can be detected. This concerns the second strip and even sometimes also the third strip (e.g. Ni04 for 1,000°C). For the next strip, the carbon content generally remains almost constant and it is equal to the initial carbon content of the alloy. The carbon content shows some variation in the Ni04 alloy oxidized at 1,000°C: this is probably a consequence of the low value of the carbon content of this alloy, which did not allow a good accuracy.

A loss of precision of the results for the alloys with low carbon contents is probably also the reason of the mismatch observed in the carbon balance sheet dressed up for the Ni02 alloy in Table 2. This table displays all the values of carbon masses in the successive strips (per cm^2 of external surface) which were deduced from the carbide fractions, using Thermo-Calc. It also shows the sum of these values for the whole analyzed area, with comparison to the initial value (i.e. before oxidation test). Surprisingly, in the case of the Ni02 alloy, which is the ternary alloy with the lowest carbon content, the carbon quantity would appear higher after oxidation than before. This is not possible with the oxidizing atmosphere which was used (no risk of carburization). On the contrary, the carbon balance sheets which were dressed up for the other samples, all showed that no carbon was lost during oxidation (Ni04 and Ni12 at 1,000°C), or only a part (Ni08 at 1,000°C and Ni12 at 1,100°C).

3.4. Consequences for the local refractoriness of the alloy

These changes in the chemical composition of the sub-surface can have consequences for the local refractoriness of the alloys. Knowing both the carbon content distribution and the chromium content, Thermo-Calc allowed calculating the distribution of local solidus temperatures. Such calculations led to the graph given in Figure 5, in which two observations can be done. First, the local enrichment in carbon between the carbide-free zone and the bulk, revealed by a coarsening of carbides, led to a local decrease in solidus temperature. Second, closer to the external surface, the impoverishment in carbon in the carbide-free zone promotes, on the contrary, a significant increase in local solidus temperature.

Furthermore, the evolution of the solidus temperature can be better described across the carbide-free zone in which the chromium content decreases from about 30% to a minimal value reached in the extreme surface. Indeed, knowing the chromium content profile obtained by WDS microprobe measurement (Figure 3), it is possible to use thermodynamic calculations in order to calculate the solidus temperature

everywhere in the carbide-free zone. However, assumptions are necessary concerning the (low) local carbon content. For example two extreme scenarios can be considered:

1. One can suppose that the carbide-free zone is saturated in carbon everywhere; this means that the carbon content is equal to the highest possible value which still allows the absence of carbides (lower than solvus), for each location in the carbide-free zone; this maximum carbon content can be determined by Thermo-Calc for each depth in the carbide-free zone (taking into account the local chromium content given by the WDS profile); knowing the contents of both chromium and carbon, Thermo-Calc can be used again for the determination of the local solidus temperature;
2. The carbon content can be considered as being negligible everywhere in the carbide-free zone (i.e. equal to zero), and then the local solidus temperatures can be calculated by Thermo-Calc only from the chromium contents given by the WDS profile across the carbide-free zone.

An example of results is given in the graph presented in Figure 6, for the Ni08 alloy oxidized at 1,000°C. From the external surface (left side of the graph) towards the bulk (right side), the solidus temperature is very high everywhere in the carbide-free zone (about 1,370°C in the hypothesis of a matrix saturated of carbon or about 1,420°C if the carbon content in matrix is equal to zero). It suddenly decreases to about 1,320°C deeper in the alloy where carbides are present again. This means that, after oxidation for 50 hours at 1,000°C, the bulk (solidus temperature of about 1315-1320°C only), is isolated from the oxidizing atmosphere by a 25µm-thick part of alloy (the carbide-free zone), the solidus temperature of which is much higher.

4. Discussion

As it is usually encountered for complex carbide-strengthened superalloys [6–8], some of the simple alloys of this study were obviously affected by a phenomenon of carbide coarsening or of precipitation of new carbides in the matrix, in a thin zone separating the carbide-free zone and the bulk. This took place at 1,000°C (or 1,100°C in one case), only for the alloys with a carbon content low enough. For the highest temperatures of oxidation test or for the alloys with more carbide, the carbon which initially belonged to the carbides in the sub-surface probably oxidized into gaseous species. It is possible that the highest temperatures and/or the highest fractions of carbides allowed, for the carbon released by the disappearing carbides, either an easier oxidation of carbon, or a diffusion of carbon over a wider area in the bulk. In the latter case, the carbide coarsening would be more diluted and then not detectable by image analysis.

One can underline that, in this study, the ternary Ni-30 wt.%Cr-xC alloys, which contain only one element easy to oxidize (Cr), allowed obtaining oxidized samples with very simple sub-surface microstructures for metallographic observations. It was possible to perform image analysis, strip by strip, in order to get a profile of carbides fraction perpendicular to the extreme surface, then a profile of carbon content across the zone affected by oxidation. Therefore, the new distribution of carbon from the external surface was easily characterized, and thereafter this allowed calculating carbon balance sheets which are more accurate or complete than previously done in previous studies [6-

8]. They showed that there are some cases for which all carbon initially belonging to the disappearing carbides (or only a part of this carbon) remain in the alloys after an inwards diffusion. However, a lack of precision of image analysis exists: it was revealed and estimated in the first part of this study [9] by the existence of a mismatch between bulk image analysis and calculations which can reach about 1% of carbide fraction. This error is nevertheless lower than the increase in carbide surface fraction which was detected between the carbide-free zone and the bulk. Since the interval of uncertainty deduced from the standard deviation is often lower than this increase in carbide surface fraction (especially for the alloys containing 0.4 to 1.2 wt.%C), quantification confirms the coarsening of carbides in the intermediate zone which was qualitatively seen the first time.

The increase in local solidus temperature in the outer part of the alloy (about 100°C more) is due to the new distribution of carbon (and also of chromium) in the zone affected by oxidation. This is potentially interesting for the heat-resistance of the alloy since the more or less deep carbide-free zone, which developed during a first exposition at high temperature, can act as a protective refractory skin for the alloy. Indeed, in case of sudden (and sufficiently short) increase in service temperature, the bulk can partially melt but it would be protected against fast oxidation, by the outer part of alloy which remains totally solid thanks to its increased solidus temperature.

Such a scenario can be illustrated by Figure 7 which presents two examples. In the first one a complex superalloy, isolated from the oxidizing atmosphere by a completely solid carbide-free zone (appeared earlier by oxidation at lower temperatures), resisted oxidation by air at 1,300°C for 20 hours although its bulk was partially molten. In the second example, another complex superalloy, the solidus temperature of which was also lower than 1,300°C, was not protected by a sufficiently thick carbide-free zone. Some molten areas were probably directly exposed to air at 1,300°C, which led to an extended oxidation which destroyed the alloy.

Thus, high temperature oxidation, which is usually considered as being a destructive phenomenon for an alloy, should be probably able, in some cases, to induce an improvement of its high temperature capabilities.

5. Conclusions

The ternary Ni-30wt.%Cr-xC alloys, with their simple microstructures and their great resistance against high temperature oxidation, are suitable to analyze the sub-surface microstructure phenomena induced by oxidation, which can also occur in more complex alloys (but in which they are more difficult to study). The inward diffusion of carbon for special sets of conditions (carbon content, temperature) was found and the new distribution of this element was precisely characterized. This was due to the cutting of sub-surface micrographs in successive strips for image analysis, and to the subsequent thermodynamic calculations. The determination of profiles of solidus temperature was also of great interest since it appeared that one of the consequences of the high temperature oxidation, the development of a carbide-free zone displaying an especially high refractoriness, may improve the heat-resistance of the alloy.

References

[1] E. F. Bradley, *Superalloys: A Technical Guide*, ASM International, 1988.
[2] C. T. Sims, W. C. Hagel, *The Superalloys*, John Wiley & Sons, 1972.
[3] S. Michon, P. Berthod, L. Aranda, C. Rapin, R. Podor, P. Steinmetz, Calphad 27 (2003) 289-294.
[4] P. Sarrazin, A. Galerie, J. Fouletier, *Les Mécanismes de la Corrosion Sèche*, EDP Sciences, 2000.
[5] P. Kofstad, *High Temperature Corrosion*, Elsevier applied science, 1988.
[6] P. Berthod, S. Michon, J. Di Martino, S. Mathieu, S. Noël, R. Podor, C. Rapin, Calphad 27 (2003) 279-288.
[7] P. Berthod, S. Michon, S. Mathieu, R. Podor, C. Rapin, P. Steinmetz, Mater. Sci. Forum 461-464 (2004) 1117-1124.
[8] P. Berthod, C. Vébert, L. Aranda, R. Podor, C. Rapin, Oxid. Met. 63 (2005) 57-72.
[9] P. Berthod, P. Lemoine, L. Aranda, submitted to Calphad.
[10] Handbook of Chemistry and Physics, 57th edition (1976-1977).
[11] Thermo-Calc version N: "Foundation for Computational Thermodynamics" Stockholm, Sweden, Copyright (1993, 2000). www.thermocalc.com
[12] NPL, unpublished work (1989).
[13] A. Dinsdale, T. Chart, MTDS NPL, Unpublished work (1986).
[14] J-O Andersson, Calphad 11 (1987) 271-276.
[15] A. Gabriel, C. Chatillon, I. Ansara, High Temperature Science 25 (1988) 17-54.

TABLES

Table 1
Example of calculation sheet for the determination of the local carbon contents from the surface fraction measured by image analysis (here Ni12 after exposure for 50h at 1,100°C)

Strip number	and **position** of this strip under the external surface **(depth in µm)**	Micrograph A **surface fraction of carbides (surf.%)** (gray level rating: 166)	Micrograph B **surface fraction of carbides (surf.%)** (gray level rating: 163)	Micrograph C **surface fraction of carbides (surf.%)** (gray level rating: 161)
0	15	*1.32* (corrected because 75% of voids and oxides)	*2.76* (corrected because 66% of voids and oxides)	*0.00* (corrected because 100% of voids and oxides)
1	45	14.77	14.76	19.23
2	75	14.88	15.37	15.95
3	105	14.26	14.90	15.44
4	135	15.39	15.27	14.67
5	165	13.77	13.51	15.67
6	195	14.52	14.71	14.76
7	225	15.96	14.84	14.16
8	255	14.50	16.26	14.27
Average value for strips 5, 6, 7 and 8:		**14.69**	**14.83**	**14.72**

Position of the strip under the external surface (depth in µm)	**Average value of the carbide fractions (surf.% or vol.%)**	Mass fraction of carbides (wt.%)	Number of moles of carbides for 100g (mol)	**Carbon Weight content (wt.%)**
15	**1.36**	1.16	0.00291	**0.1286**
45	**16.25**	14.23	0.03557	**1.3389**
75	**15.40**	13.46	0.03366	**1.2660**
105	**14.87**	12.99	0.03247	**1.2208**
135	**15.11**	13.21	0.03302	**1.2417**
165	**14.32**	12.50	0.03125	**1.1746**
195	**14.66**	12.81	0.03202	**1.2038**
225	**14.99**	13.10	0.03274	**1.2310**
255	**15.01**	13.12	0.03280	**1.2333**

Table 2
Values of carbon calculated with Thermo-Calc for each strip; balance sheets of the whole areas for the five studied samples

Strip number	**Ni02 after 50h at 1,000°C**		**Ni04 after 50h at 1,000°C**		**Ni08 after 50h at 1,000°C**	
	C content in the strip (wt.%)	C mass per unit of external surface (mg/cm^2)	C content in the strip (%wt.)	C mass per unit of external surface (mg/cm^2)	C content in the strip (%wt.)	C mass per unit of external surface (mg/cm^2)
0	0.443	0.108	0.203	0.050	0.000	0.000
1	0.829	0.202	0.547	0.133	0.659	0.161
2	0.327	0.080	0.498	0.121	0.788	0.192
3	0.245	0.060	0.351	0.086	0.790	0.193
4	0.328	0.080	0.385	0.094	0.847	0.206
5	0.199	0.049	0.412	0.100	0.780	0.190
6	0.238	0.058	0.429	0.105	0.810	0.197
7	0.188	0.046	0.422	0.103	0.783	0.191
8	0.160	0.039	0.348	0.085	0.864	0.211
Final mass of C*	**0.720mg per cm^2** of ext. surf.		**0.876mg per cm^2** of ext. surf.		**1.540mg per cm^2** of ext. surf.	
comparison:	>		≈		≈	
Initial mass of C**	**0.438mg per cm^2** of ext. surf.		**0.877mg per cm^2** of ext. surf.		**1.754mg per cm^2** of ext. surf.	

Strip number	**Ni12 after 50h at 1,000°C**		**Ni12 after 50h at 1,100°C**		
	C content in the strip (wt.%)	C mass per unit of external surface (mg/cm^2)	C content in the strip (wt.%)	C mass per unit of external surface (mg/cm^2)	
0	0.514	0.125	0.129	0.031	*: total mass of carbon per unit of external surface, which is still present in the whole analyzed area after oxidation (i.e. strips 0 to 8 together).
1	1.424	0.347	1.339	0.326	
2	1.226	0.299	1.266	0.308	
3	1.231	0.300	1.221	0.297	
4	1.179	0.287	1.242	0.302	
5	1.208	0.294	1.175	0.286	**: total mass of carbon per unit of external surface, which was initially present in the same whole area (i.e. strips 0 to 8 together).
6	1.178	0.289	1.204	0.293	
7	1.178	0.287	1.231	0.300	
8	1.265	0.308	1.233	0.300	
Final mass of C*	**2.536mg per cm^2** of ext. surf.		**2.445mg per cm^2** of ext. surf.		
comparison:	≈		≈		
Initial mass of C**	**2.631mg per cm^2** of ext. surf.		**2.631mg per cm^2** of ext. surf.		

FIGURES

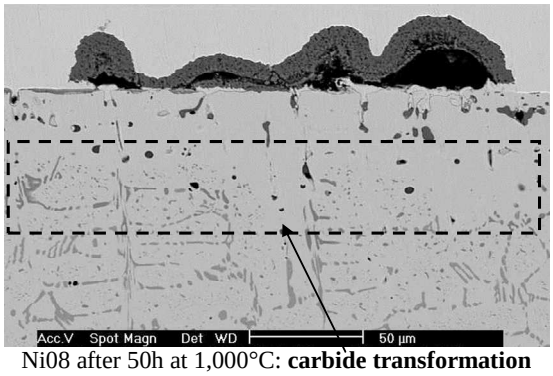

Ni08 after 50h at 1,000°C: **carbide transformation**

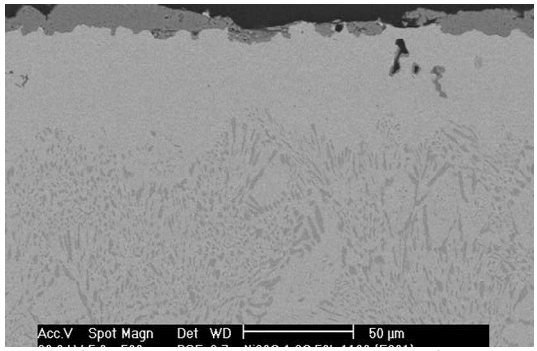

Ni16 after 50h at 1,100°C: no carbide transformation

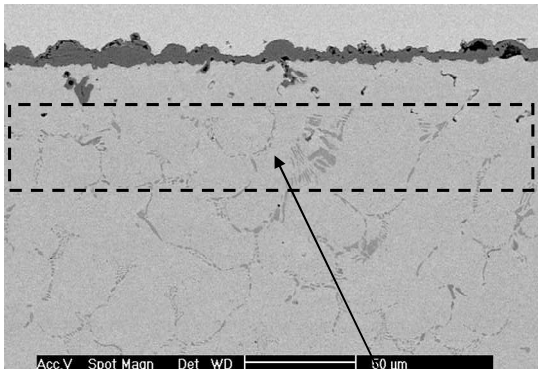

Ni04 after 50h at 1,000°C: **carbide transformation**

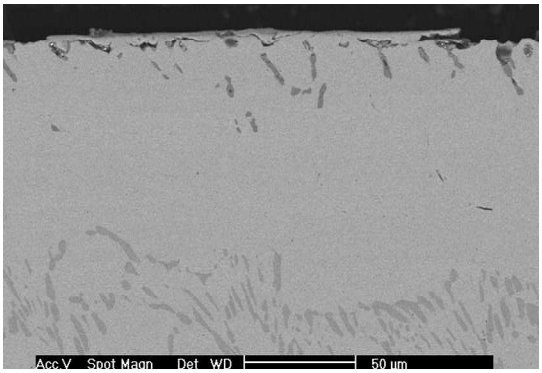

Ni12 after 50h at 1,200°C: no carbide transformation

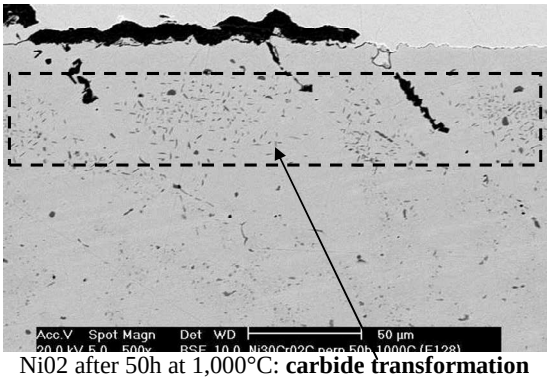

Ni02 after 50h at 1,000°C: **carbide transformation**

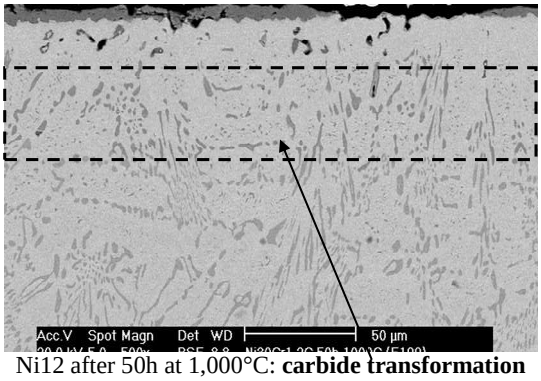

Ni12 after 50h at 1,000°C: **carbide transformation**

Fig. 1. Four examples of sub-surface microstructures of oxidized carbides-containing nickel-based alloys, displaying carbides transformations along the carbide-free zone, and, for comparison, and two examples for which such phenomena did not occur (pictures taken with SEM in BSE mode)

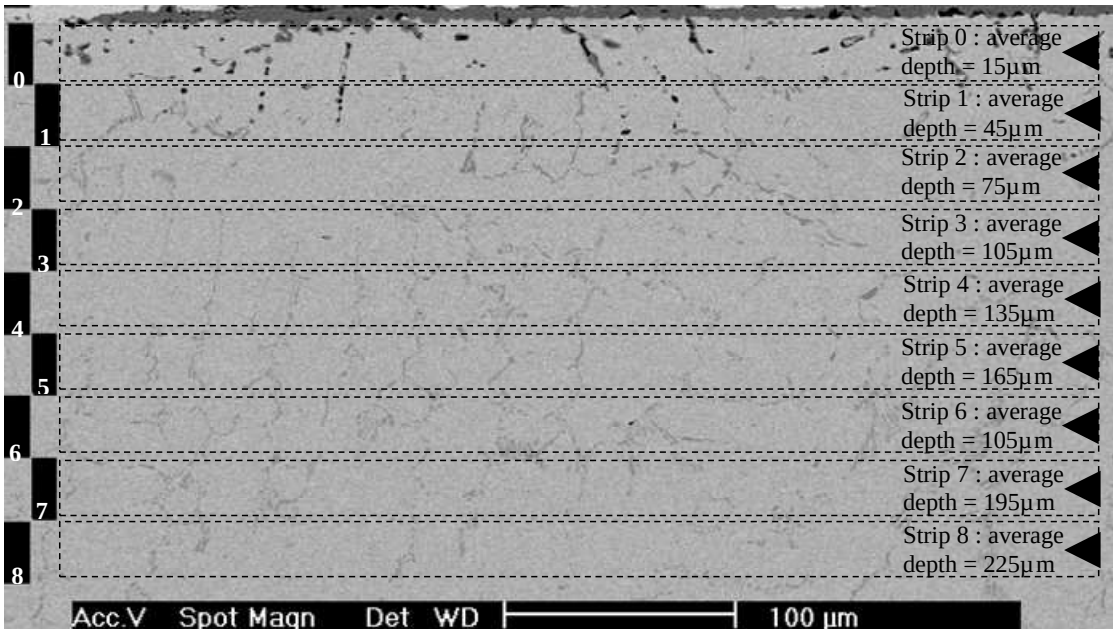

Strip N°0 : d=0 to 30µm (no carbides, internal oxides)	9.00%
Strip N°1 : d=30 to 60µm (average d = 45µm)	5.33%
Strip N°2 : d=60 to 90µm (average d = 75µm)	4.28%
Strip N°3 : d=90 to 120µm (average d = 105µm)	3.23%
Strip N°4 : d=120 to 150µm (average d = 135µm)	3.96%
Strip N°5 : d=150 to 180µm (average d = 165µm)	4.33%
Strip N°6 : d=180 to 210µm (average d = 195µm)	6.04%
Strip N°7 : d=210 to 240µm (average d = 225µm)	4.50%
Strip N°8 : d=240 to 270µm (average d = 255µm)	3.33%
The successive cut strips (magnitude divided by 2 compared to the initial micrograph (top)	Corresponding digitalized pictures and value of the number fraction of black pixels (gray level = 155)

Division in 8 strips of a SEM/BSE micrograph of a sub-surface displaying carbides modifications (here Ni04 1,000°C); partitioning of the pixels between white and black for the value of gray level leading, for the strips N°5 to 8, to an average surface fraction close to the 4.95% given by Thermo-Calc; values of the black pixels number fractions (carbides, or internal oxides in the case of the band N°0) obtained by image analysis

Fig. 2. Illustration of the method which was applied for obtaining the evolution of the surface carbide fraction

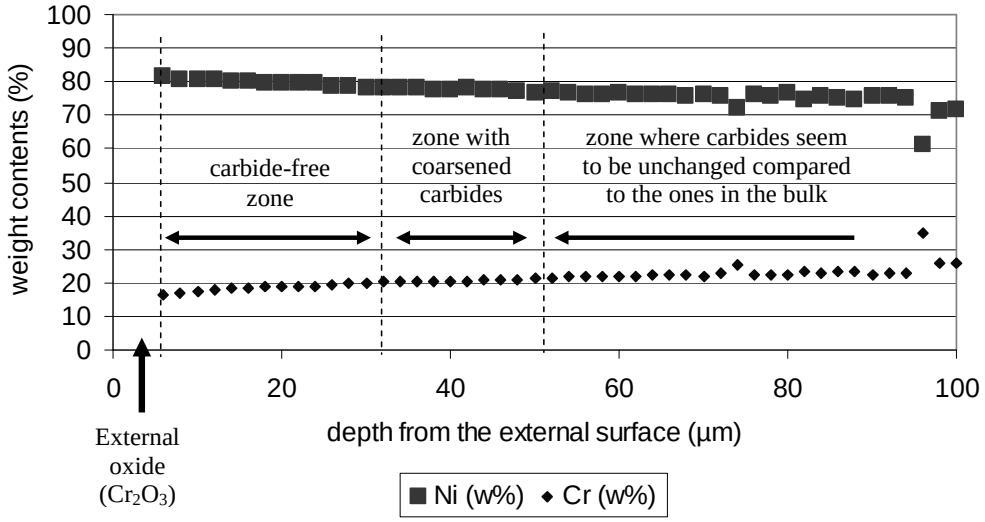

Fig. 3. Example of a weight chromium content profile across the sub-surface of an oxidized sample (here Ni08 1,000°C); positions of the different metallurgical zones seen with the SEM

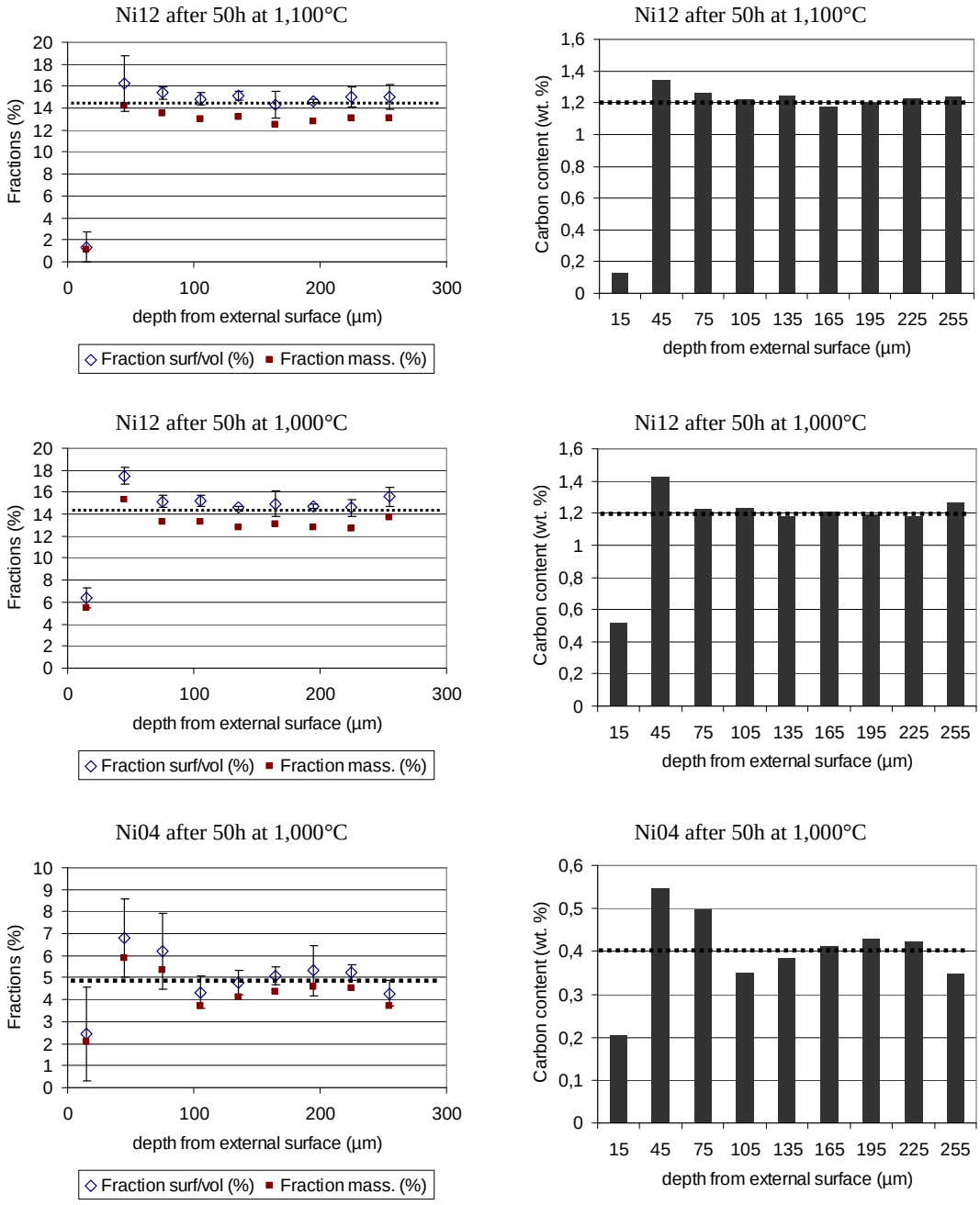

Left: evolution, versus the depth, of the measured surface or volume fraction of carbides (average ± standard deviation); comparison with the bulk (horizontal dotted line), and evolution of the corresponding mass fraction;
Right: evolution of the carbon content deduced from the carbide mass fractions using Thermo-Calc, with comparison to the alloy carbon content (horizontal dotted line)

Fig. 4. Evolution of the carbides fractions and of the corresponding carbon contents for three different samples

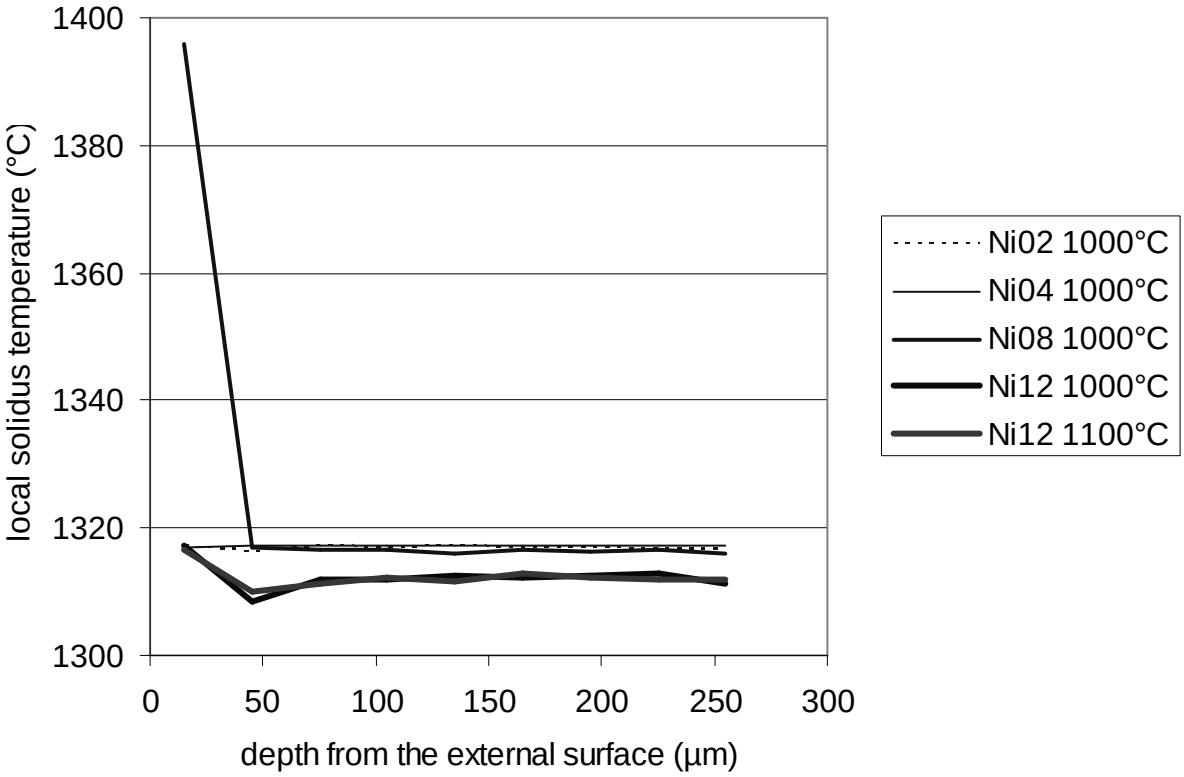

Fig. 5. Evolution of the local solidus temperature calculated by Thermo-Calc from the carbon profiles over the whole sub-surface area where the carbides fractions were measured

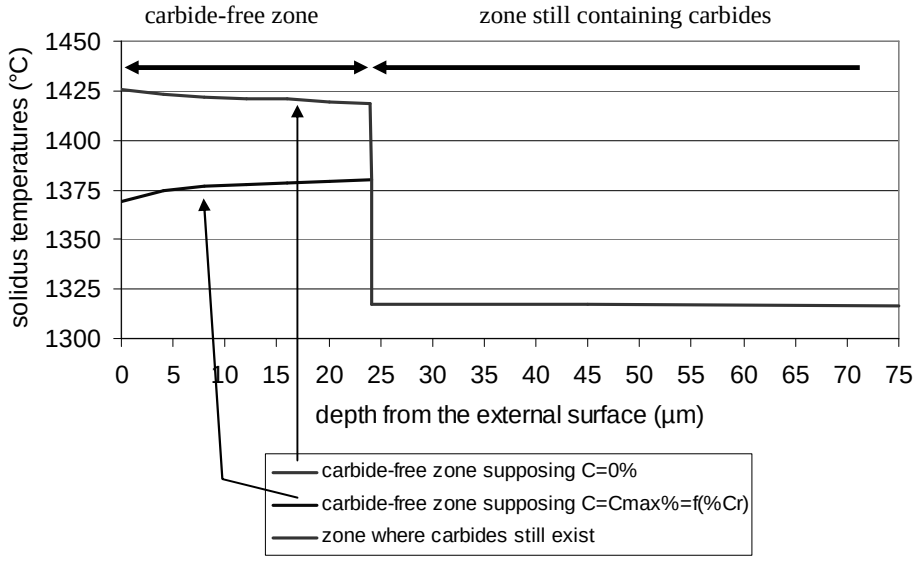

Fig. 6. Evolution, in the sub-surface of Ni08 oxidized at 1,000°C, of the local solidus temperature calculated by Thermo-Calc from the chromium profile (Figure 3) for the carbide-free zone, and for 30 wt.%Cr and the calculated carbon contents (Table 3) for the deeper zone which still contains carbides

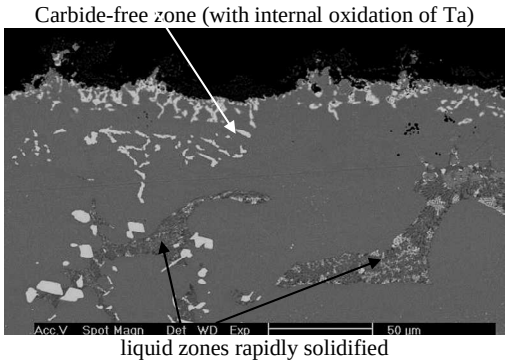

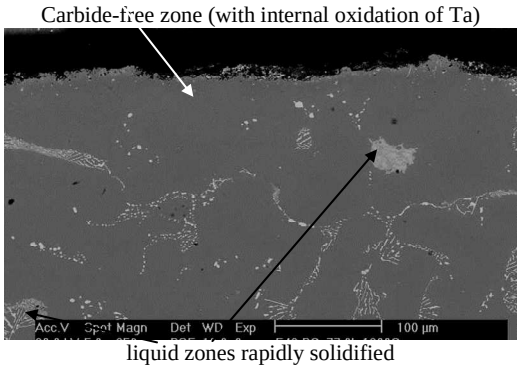

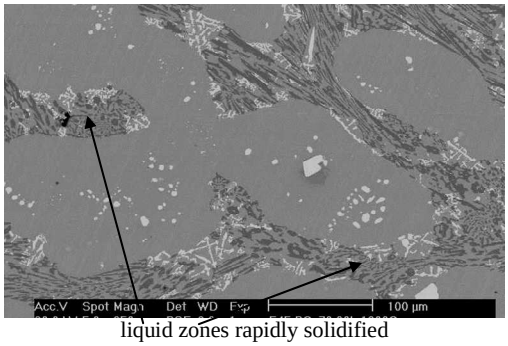

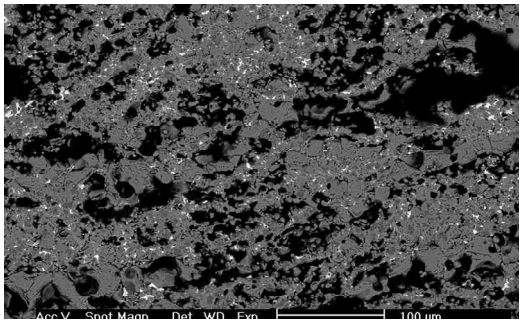

Superalloy 1
($T_{beginning\ of\ fusion}$ < 1,300°C)

Superalloy 2
($T_{beginning\ of\ fusion}$ < 1,300°C)

(* molten zones are clearly visible since the rapid solidification by quenching in water led to very fine microstructures
in the interdendritic zones)

Fig. 7. Superalloy 1 (left): probable protection of the bulk, by the carbide-free zone developed during heating (and still solid thanks to its increased refractoriness), avoiding a fast oxidation of the interdendritic molten zones; Superalloy 2 (right): no such protection since catastrophic oxidation occurred in the whole alloy